BIOCHEMISTRY
including biophysical chemistry & molecular biology

ARTICLE

pubs.acs.org/biochemistry

Treponema denticola PurE Is a Bacterial AIR Carboxylase

Sylvain Tranchimand,[†] Courtney M. Starks,[‡] Irimpan I. Mathews,[§] Susan C. Hockings,[‡] and T. Joseph Kappock*[,†]

[†]Department of Biochemistry, Purdue University, West Lafayette, Indiana 47907-2063, United States

[‡]Department of Chemistry, Washington University, St. Louis, Missouri 63130, United States

[§]Stanford Synchrotron Radiation Lightsource, 2575 Sand Hill Road, Menlo Park, California 94025, United States

Supporting Information

ABSTRACT: De novo purine biosynthesis proceeds by two divergent paths. In bacteria, yeasts, and plants, 5-aminoimidazole ribonucleotide (AIR) is converted to 4-carboxy-AIR (CAIR) by two enzymes: N^5-carboxy-AIR (N^5-CAIR) synthetase (PurK) and N^5-CAIR mutase (class I PurE). In animals, the conversion of AIR to CAIR requires a single enzyme, AIR carboxylase (class II PurE). The CAIR carboxylate derives from bicarbonate or CO_2, respectively. Class I PurE is a promising antimicrobial target. Class I and class II PurEs are mechanistically related but bind different substrates. The spirochete dental pathogen *Treponema denticola* lacks a *purK* gene and contains a class II *purE* gene, the hallmarks of CO_2-dependent CAIR synthesis. We demonstrate that *T. denticola* PurE (*Td*PurE) is AIR carboxylase, the first example of a prokaryotic class II PurE. Steady-state and pre-steady-state experiments show that *Td*PurE binds AIR and CO_2 but not N^5-CAIR. Crystal structures of *Td*PurE alone and in complex with AIR show a conformational change in the key active site His40 residue that is not observed for class I PurEs. A contact between the AIR phosphate and a differentially conserved residue (*Td*PurE Lys41) enforces different AIR conformations in each PurE class. As a consequence, the *Td*PurE·AIR complex contains a portal that appears to allow the CO_2 substrate to enter the active site. In the human pathogen *T. denticola*, purine biosynthesis should depend on available CO_2 levels. Because spirochetes lack carbonic anhydrase, the corresponding reduction in bicarbonate demand may confer a selective advantage.

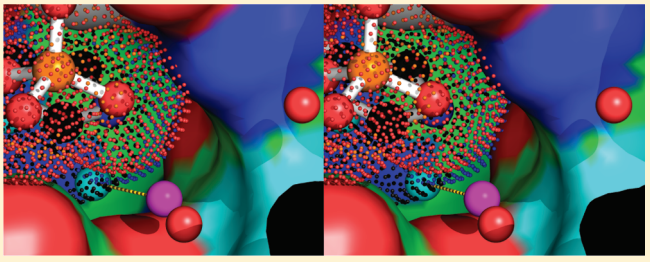

The central reactions of de novo purine biosynthesis represent an unusual example of metabolic diversification, most obviously in the eukaryotes. Animals convert 5-aminoimidazole ribonucleotide (AIR), the first pathway heterocycle, to 4-carboxy-AIR (CAIR) by a route different from that used by yeasts or plants.[1] Bacteria, yeasts, and plants contain two enzymes. PurK (N^5-CAIR synthetase, EC 6.3.4.18) converts AIR, bicarbonate, and ATP to N^5-carboxy-AIR (N^5-CAIR), ADP, and inorganic phosphate (P_i). Next a class I PurE (N^5-CAIR mutase, EC 5.4.99.18) reversibly converts the chemically labile N^5-CAIR to CAIR (Figure 1).[2] Yeast and plant ADE2s are PurK−class I PurE fusion proteins.[3,4] A separate enzyme, PurC (EC 6.3.2.6), converts CAIR, ATP, and L-Asp to 4-(*N*-succinylcarboxamide)-AIR, ADP, and P_i.[5,6]

N^5-CAIR has no known role in de novo purine biosynthesis in animals, all of which lack recognizable *purK* genes. Instead, animals contain a class II PurE (AIR carboxylase, EC 4.1.1.21) that converts AIR and CO_2 to CAIR and a proton.[5] Animal class II PurEs are found in PurC−PurE fusion proteins, known as PAICS.[7] Eukaryotic purine biosynthesis pathways may have diverged because environmental conditions favor one PurE class over the other.[8]

Despite their differing substrate preferences, class I and II PurEs are thought to use similar reaction chemistries.[8] A ternary

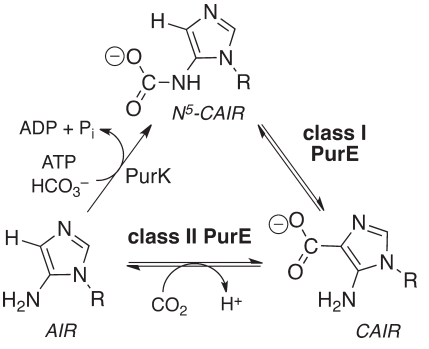

Figure 1. Different routes from AIR to CAIR. Note that the C_1 donor differs in each route. R is ribose 5′-phosphate.

PurE·AIR·CO_2 complex is a proposed intermediate in the class I reaction, and it is the Michaelis complex for the class II reaction. PurE classes are distinguished by differentially conserved sequences in the 40s and 70s loops (Figure 2).[9] Biochemical data

Received: December 21, 2010
Revised: April 26, 2011
Published: May 06, 2011

Figure 2. Alignment of the PurE 40s and 70s loops. *Td*PurE numbering is used. Universally conserved residues have black backgrounds. Highly conserved, class-specific ("differentially conserved") residues are boxed. Human and chicken PAICS PurE domains (HumanE and ChickE) have identical sequences in these loops. Organism codes: *Td*, *Treponema denticola*; *Af*, *Archaeoglobus fulgidus*; *Aa*, *Acetobacter aceti*; *Ec*, *Escherichia coli*.

and crystal structures, including several with bound nucleotides, are available for several class I PurEs.[9−12] Less biochemical data are available for class II PurEs.[1,7] A structure of human PAICS crystallized in the absence of organic ligands has been determined at modest resolution.[13]

Treponema denticola is a cultivable, anaerobic spirochete that resides in dental plaque biofilms and contributes to persistent human periodontal disease.[14−16] Most spirochetes are fastidious and lack de novo purine biosynthesis genes.[17−19] However, the *T. denticola* genome[20] contains a full set of 10 de novo purine pathway genes (Table S1 of the Supporting Information), including a class II PurE (*Td*PurE). This is most unusual in prokaryotes; the first microbial class II PurE was identified in the euryarchaeote *Archaeoglobus fulgidus*.[8] Neither organism contains a recognizable *purK* gene, which accompanies class I *purE* genes.[a] Prokaryotic PurE forms are monofunctional, unlike fungal and plant ADE2 (class I PurE domain) or animal PAICS (class II PurE domain).

Here we show that *Td*PurE is a bona fide class II PurE. The pH dependence of CAIR decarboxylation is different in each PurE class, consistent with different proton transfer mechanisms. Crystal structures show few class-specific differences in polar contacts with bound AIR. However, the AIR conformation is different in each class and appears to determine if CO_2 can be sequestered from solvent. A physiological implication is that purine biosynthesis in *T. denticola* should depend strictly on CO_2 levels.

EXPERIMENTAL PROCEDURES

Materials and Methods. Restriction enzymes, Vent DNA polymerase, DNA-modifying enzymes, and DNA size standards were obtained from NEB. Cloned Pfu DNA polymerase was from Stratagene. All other reagents were from Sigma-Aldrich or Fisher Scientific. Oligodeoxynucleotides (Table S2 of the Supporting Information) were obtained from IDT and used without further purification. Spectra and kinetic progress curves were recorded on a Beckman DU640 spectrophotometer equipped with a thermostated cell holder. Protein concentrations were measured using a Bio-Rad Bradford assay with crystalline bovine serum albumin as the standard.[21] Total $[CO_2 + HCO_3^-]$, $[CO_2]_T$, was measured using an L3K CO_2 quantitation kit (Genzyme Diagnostics). Analytical gel filtration was performed using a calibrated column at 5 °C using 20 mM Tris-HCl (pH 8.0) and 100 mM NaCl as described previously.[11] *Escherichia coli* PurK (*Ec*PurK; 43 units mg^{-1} at 37 °C and 28 units mg^{-1} at 30 °C, each at pH 8.0) was isolated from autoinduced pNC2/BL21(DE3) cells as described previously.[6,8] *E. coli* PurC with an N-terminal hexa-His tag (*Ec*PurC; 16 units mg^{-1} at 37 °C) was expressed and purified from a pET22b-derived vector as described previously.[22] CAIR was synthesized by Hong Jiang from 5-aminoimidazole-4-carboxamide ribonucleotide as described previously.[1,23]

AIR was prepared by enzyme-mediated CAIR decarboxylation. A final volume of 50 μL containing 50 mM Tris-HCl (pH 8.0), ∼5 μmol of CAIR, and 24 μg of *Td*PurE was incubated at 30 °C for 30 min. *Td*PurE was removed by centrifugal ultrafiltration (30 min at 14000*g*) using a Microcon Ultracel YM-10 device (Millipore).

Sequence Alignments and Phylogenetic Analysis. PurE and PurE domain sequences were selected from a phylogenetically diverse set of organisms listed in the Supporting Information. ClustalW[24] implemented within MEGA4[25] was used to align protein sequences with pairwise and multiple-alignment penalties of 35 and 15 for gap opening and 0.75 and 0.3 for gap extension, respectively. CodonAlign 2.0 was used to create DNA sequence alignments templated by these protein alignments (codon-aligned DNA), which improves gap placements and thereby tree quality.[26] Phylogenetic analyses were performed with complete gap deletion, considering only the first and second positions of each codon to correct for interspecific differences in base composition. Start codons for all full-length DNA sequences were set to ATG.

MEGA4 was used to perform neighbor-joining (NJ) phylogenetic analyses using a bootstrap test with 1000 replicate trees to test the inferred phylogeny.[27,28] NJ protein analyses were performed with Poisson correction to compute evolutionary distances in units of amino acid changes per site.[29] Maximum-likelihood (ML) phylogenetic analyses[30] of codon-aligned DNAs were performed with PhyloWin 2.0[31] using 1000 bootstrap replicates.

Gene Construction. A synthetic gene encoding *T. denticola* ATCC 35405 PurE (GenBank accession number AAS11180) was used to create plasmid pJK376 (Appendix 1 of the Supporting Information). QuikChange mutagenesis of plasmid pJK376 using oligodeoxynucleotides 1316 and 1317 furnished plasmid pJK392, encoding H40N-*Td*PurE.

Protein Expression and Purification. A starter culture of *E. coli* BL21(DE3) cells transformed with pJK376 (or pJK392 for H40N-*Td*PurE) was grown overnight at 37 °C in noninducing MDG medium[34] containing 50 mg L^{-1} ampicillin. The starter culture was then used at a 1:100 dilution to inoculate 1 L production cultures in autoinduction medium ZYM-5052[32] containing 50 mg L^{-1} ampicillin in 2.8 L Fernbach flasks. The cultures were grown at 37 °C for 4.5 h and then overnight at 16 °C. Cells were harvested by centrifugation and then used immediately or stored at −80 °C. All subsequent steps were performed at 4 °C.

Cells (5−27 g) were resuspended in lysis buffer [>5 mL/g of cell paste; 50 mM Tris-HCl (pH 8.0) and 100 mM potassium chloride] and lysed by sonication (3 × 30 s, with 1 min cooling intervals). The lysate was cleared by centrifugation (30000*g* for 30 min), and the supernatant was adjusted to 1% streptomycin from a 10% (w/v) stock. Solids were removed by centrifugation (30000*g* for 15 min). Ammonium sulfate (390 g/L) was added to the supernatant over a period of 30 min to reach 60% saturation. After the mixture had been stirred for a further 30 min, solids were then removed by centrifugation (30000*g* for 15 min). The supernatant was then applied to a column of Phenyl Sepharose 6 Fast Flow resin (2.5 cm × 7.5 cm, GE Healthcare) equilibrated in buffer A [20 mM Tris (pH 8.0) and 1.5 M ammonium sulfate]. The column was washed with buffer A and then developed with a

linear gradient (300 mL × 300 mL) of buffer A to buffer B [20 mM Tris (pH 8.0)]. Fractions containing *Td*PurE were pooled, dialyzed against buffer B, and loaded onto a column of hydroxyapatite Bio-Gel HT (2.5 cm × 3 cm, Bio-Rad) that was equilibrated in buffer C [10 mM potassium phosphate (pH 8.0)]. The column was washed with buffer C and then developed with a linear gradient (100 mL × 100 mL) of buffer C to buffer D [500 mM potassium phosphate (pH 8.0)]. Fractions containing *Td*PurE were pooled and concentrated to >5 mg mL^{-1} using Amicon Ultra (molecular weight cutoff of 30000) or Centricon YM10 concentrators. Concentrated protein was applied to a Superdex 200 column (1.6 mL × 60 mL, GE Healthcare) equilibrated in lysis buffer. Fractions containing *Td*PurE were pooled, concentrated, and exchanged into 5 mM Tris (pH 8.0) and 20 mM KCl using Amicon Ultra concentrators. Purified *Td*PurE was then stored in small aliquots at −80 °C.

Steady-State Kinetic Analysis. A unit is the amount of enzyme that forms 1 μmol of product per minute under the specified conditions. Kinetic constants were obtained by nonlinear least-squares fitting to the Michaelis−Menten equation with Kaleidagraph 3.6 (Synergy Software) or SigmaPlot 10.0 (Systat Software).

End Point Assay for AIR Quantitation. A final volume of 0.5 mL containing 50 mM Tris-HCl (pH 8.0), 5 mM $MgCl_2$, 2 mM phosphoenolpyruvate (PEP, sodium salt), 1 unit of pyruvate kinase (rabbit muscle), 5 mM aspartic acid, 50 μM ATP, 20 mM $KHCO_3$, 0.1 unit of *Ec*PurC, and variable amounts of AIR (10−100 μM) was incubated at 37 °C. The reaction was initiated by the addition of 1 unit of *Td*PurE, and the differential absorbance at 282 nm due to formation of 4-(*N*-succinylcarboxamide)-AIR ($\Delta\varepsilon_{282}$ = 8.48 mM^{-1} cm^{-1}) was used to quantitate AIR.[7]

*CAIR Decarboxylation Assay. Td*PurE was assayed in the reverse biosynthetic direction (CAIR → AIR) by a published method.[6] A stoppered, masked, 1 cm path length cuvette containing 50 mM Tris-HCl (pH 8.0) and variable amounts of CAIR (1.5−150 μM) in a final volume of 0.5 mL was incubated at either 10 or 30 °C for >5 min. Reactions were initiated by the addition of *Td*PurE (24−47 ng mL^{-1}; 1.4−2.8 nM subunits). The initial velocity of CAIR decomposition (<10% conversion of CAIR; $\Delta\varepsilon_{260}$ = 8.93 mM^{-1} cm^{-1}) was recorded at 260 nm, with a correction for a small background slope. A version of this assay with 47 μg mL^{-1} *Td*PurE was used to quantitate CAIR at 30 °C.

*High-Bicarbonate AIR Carboxylation Assay. Td*PurE was assayed in the forward biosynthetic direction (AIR → CAIR) by a published method.[7] A final volume of 0.5 mL containing 50 mM Tris-HCl (pH 8.0), 200 mM $KHCO_3$, and variable amounts of AIR (10−130 μM) was incubated at 30 °C for >5 min. The reaction was initiated by the addition of 1 μg of *Td*PurE (subunit concentration of 120 nM), and the initial velocity of CAIR formation was determined as described for the CAIR decarboxylation assay.

pH Dependence of CAIR Decarboxylation. A three-component buffer system (100 mM Tris-HCl, 50 mM MES, and 50 mM acetic acid) was used within the pH range of 5.5−9.5 at a constant ionic strength of 0.1 M.[33] A final volume of 0.5 mL containing variable amounts of CAIR (2−100 μM) was incubated at 30 °C for 3 min prior to the addition of *Td*PurE to a final concentration of 1.1 nM to initiate the reaction. Initial velocities were computed using $\Delta\varepsilon_{260}$ values measured for the CAIR → AIR conversion at each pH after correcting for nonenzymatic decarboxylation.[11] In only one instance was the background rate >11% of the corrected decarboxylase velocity (18% at pH 5.5 and the highest CAIR concentration used).

Nonlinear least-squares fits of the pH-dependent parameter k_{cat}/K_m to eq 1 yielded the corresponding pH-independent parameter $\tilde{k}_{cat}/\tilde{K}_m$. The corresponding k_{cat} data were fit using eq 2, an expression for product formation via two enzyme−substrate complexes. The derivation of eq 2 is given in Appendix 2 of the Supporting Information.

$$\log \frac{k_{cat}}{K_m} = \log\left(\frac{\tilde{k}_{cat}/\tilde{K}_m}{1+\dfrac{[H^+]}{K_{a1}}+\dfrac{K_{a2}}{[H^+]}}\right) \quad (1)$$

$$\log k_{cat} = \log\left(\frac{\dfrac{\tilde{k}_1[H^+]}{K_{a1}}+\tilde{k}_2}{1+\dfrac{[H^+]}{K_{a1}}+\dfrac{K_{a2}}{[H^+]}}\right) \quad (2)$$

Forms of eqs 1 and 2 in which the independent variable and fitted parameters were replaced with logarithmic values (e.g., 10^{-pH} in place of $[H^+]$) were used to obtain uncertainties for pK_a parameters.

Steady-State Distribution of Products Formed from CAIR by PurE in the Presence of *Ec*PurK. The use of an N^5-CAIR regeneration system including *Ec*PurK is described in Appendix 3 of the Supporting Information. A final volume of 0.85 mL in a stoppered cuvette (minimal headspace) containing 50 mM Tris-HCl (pH 8.0), 50 mM $KHCO_3$, 0.5 mM $MgCl_2$, 2 mM creatine phosphate, 50 μM ATP, 44 μM CAIR, 1 unit of creatine kinase (rabbit muscle; Boehringer Mannheim), and 0.28 unit of *Ec*PurK (0.3 μM) was incubated at 30 °C for 3 min. The ultraviolet absorption spectrum was recorded, and then 0.07 unit of either *Ec*PurE or *Td*PurE was added. The final absorption spectrum was recorded after incubation for an additional 3 min. (Control experiments lacking *Ec*PurK required a 30 min incubation after the addition of PurE.)

Pre-Steady-State Reactions of CO_2 with AIR in the Presence of PurE. The ability of *Td*PurE to use CO_2 as a substrate was assessed by initiating AIR carboxylation with the addition of CO_2-enriched water.[7] The initial velocity was recorded within the first 30 s, i.e., before the CO_2−HCO_3^- equilibrium becomes established. The CO_2 solution was prepared by continuous bubbling of CO_2(g) into water at 10 °C, yielding 48 g L^{-1} CO_2.[34]

The qualitative dependence of the AIR → CAIR reaction performed by each PurE on CO_2 was assessed at 10 °C at high enzyme concentrations. A final volume of 0.5 mL in a stoppered cuvette containing 50 mM Tris-HCl (pH 8.0), 100 μM AIR, and variable amounts of either *Td*PurE (0.059−0.23 unit, measured using the CAIR decarboxylation assay at 10 °C; 2.4−9.4 μg mL^{-1}) or *Ec*PurE (0.14−0.56 unit, measured using the CAIR decarboxylation assay at 10 °C; 30−120 μg mL^{-1}) was incubated at 10 °C for 5 min. CO_2 was added from a saturated solution to an initial concentration of 20 mM, and the progress curve at 260 nm was recorded. The value of $[CO_2]_T$ measured using a kit in equilibrated reaction mixtures was taken to be the initial $[CO_2]$.

The determination of kinetic constants was performed with *Td*PurE. A final volume of 0.5 mL in a stoppered cuvette containing 50 mM Tris-HCl (pH 8.0), a variable amount of AIR (30−600 μM), and 0.12 unit of *Td*PurE (measured using

the CAIR decarboxylation assay at 10 °C; 4.7 μg mL^{-1}, 0.28 μM subunits) was incubated at 10 °C for 5 min. The reaction was initiated by adding variable amounts of a saturated CO_2 solution (0.5−30 mM initial CO_2 concentration in the reaction mixture), and the progress curve at 260 nm was recorded.

Progress curves were fit to eq 3

$$A_{260} = A_0 + A_1[1 - \exp(-k_1 t)] + A_2 t \quad (3)$$

where A_0 is the absorbance reading prior to the addition of CO_2, A_1 is the differential increase in absorbance due to CAIR formation, and A_2 approximates the initial portion of the slow, complex approach to AIR−N^5-CAIR−CAIR equilibrium, which occurs as the CO_2−HCO_3^- equilibrium is established. The derivative of eq 3 is eq 4

$$\frac{dA_{260}}{dt} = A_1 k_1 \exp(-k_1 t) + A_2 \quad (4)$$

Initial velocities (i.e., at $t \rightarrow 0$) were computed using eq 5

$$v = \frac{A_1 k_1}{\Delta\varepsilon_{260}/V} \quad (5)$$

where $\Delta\varepsilon_{260}/V$ = 17.9 μmol^{-1} for a 0.5 mL reaction in a 1 cm path length cuvette.

Crystallization and Data Collection. *Td*PurE crystals were grown at room temperature by the hanging drop vapor diffusion method. Drops consisted of 1 μL of protein solution and 1 μL of reservoir solution. Reservoirs contained 0.5 mL of 14−16% (w/v) PEG 1000, 100 mM $MgCl_2$, and 100 mM imidazole (pH 8.0). Cube-shaped crystals grew over several days. For the uncomplexed structure, a crystal was quickly dipped into a cryoprotectant solution containing 20% (v/v) ethylene glycol, 22% PEG 1000, 200 mM $MgCl_2$, and 100 mM imidazole (pH 8.0). The crystal was then flash-cooled in liquid N_2.[35] Diffraction data were collected at Advanced Light Source beamline 4.2.2 and indexed, integrated, and scaled using d*TREK.[36]

A *Td*PurE crystal was soaked for 1.5 h in a solution containing 0.5 mM CAIR, 16% (w/v) PEG 1000, 100 mM $MgCl_2$, and 100 mM imidazole (pH 8.0); the crystal was then quickly dipped in the same solution with 20% (v/v) ethylene glycol and flash-cooled in a N_2 stream at 110 K. Diffraction data were collected on a Rigaku R-Axis IV image plate detector using a graphite-monochromated Cu Kα X-ray beam from a Rigaku RU200 generator operated at 5 keV. Data were indexed, integrated, and scaled with d*TREK.

Determination and Refinement of Structure. The structure of *Td*PurE was determined by molecular replacement using the *Thermotoga maritima* PurE octamer [Protein Data Bank (PDB) entry 1o4v][37] as the search model. The C-terminal helix was removed, and side chains were pruned using the MINI command in SEAMAN.[38] A solution was found with MOLREP,[39] using space group $P2_1$ with the octamer as the search model. To avoid bias introduced by the high degree of noncrystallographic symmetry (NCS), the test set for R_{free} calculation was selected in thin resolution shells. The molecular replacement solution was first refined against the data set from the CAIR-soaked crystal (using the same test set chosen for the uncomplexed crystal). Rigid-body refinement, simulated annealing, and grouped *B* factor refinement were performed in CNS[40] using strict NCS constraints. Additional refinement, and manual rebuilding with O,[41] were then conducted; subsequent rounds of refinement and addition of water were conducted in REFMAC5[42] with ARP/wARP,[43] using tight NCS restraints. The protein portion of the resulting *Td*PurE·AIR complex was then refined against the data set from the uncomplexed crystal; refinement and addition of water were conducted in REFMAC5 with ARP/wARP, using tight NCS restraints, and manual adjustment of the model was conducted in O. While the resulting *Td*PurE model was consistent with composite omit maps calculated using CNS, refinement stalled at high values of the refinement statistics (R and R_{free} values of 25.8 and 29.7%, respectively, for *Td*PurE). The H test statistics[44] in the CTRUNCATE[45] output suggested a twinning fraction of 0.23 (Table 2).

Both data sets were reprocessed using XDS,[46] using the same R_{free} test sets, which gave improved statistics. Twin refinement performed in REFMAC5[47] significantly improved refinement statistics for the stalled *Td*PurE model. We performed several cycles of refinement followed by model rebuilding and addition of water in COOT,[48] guided by $2F_o - F_c$ and $F_o - F_c$ electron density maps and hydrogen bonding interactions. NCS restraints were removed in the final stages of refinement. Data collection and refinement statistics are listed in Table 2.

The data set obtained from the CAIR-soaked crystal (*Td*PurE·AIR complex) was indexed in the $P2_1$ and $C222$ space groups. Because CTRUNCATE analysis did not suggest twinning, we attempted to determine the structure in the $P2_1$, $C222$, and $C222_1$ space groups. MOLREP gave solutions for both $P2_1$ (an octamer) and $C222_1$ (a tetramer), using a monomer of the native *Td*PurE as the search model. However, the $C222_1$ solution was refined with better statistics. AIR was built into electron density present in each active site in the asymmetric unit. A carbamate was modeled at the N-terminus of one chain. Iterative refinement of the final *Td*PurE·AIR model was performed as described above.

Structure Analysis and Figure Production. Calculations of root-mean-square differences between protein models were conducted in LSQMAN.[49] Electron density maps for PAICS were calculated with CCP4 programs,[45] using the structure factors and model from PDB entry 2h31. This model contains one CO_2 molecule, with an occupancy of 0.5 for the C atom, and an occupancy of 1.0 for each oxygen atom. However, because the carbon atom is on the 2-fold axis, this results in an occupancy of 2.0 for each oxygen atom. The occupancy of the CO_2 molecule was therefore changed to 0.5 prior to calculation of phases from the model. Figures were prepared using PyMOL[50] or ESPript 2.2.[51]

RESULTS

Sequence Analysis. A complete set of 10 purine biosynthesis enzymes is present in *T. denticola*, apart from the PurS component of the multimeric formylglycinamidine ribonucleotide synthase (EC 6.3.5.3; Table S1 of the Supporting Information). BLASTP searches failed to identify a PurK homologue, as expected for an organism that contains a class II PurE.[b]

*Td*PurE protein and DNA sequences were compared with those of a diverse group of PurEs, identified as class I or class II by characteristic sequences in the 40s and 70s loop regions (Figure 2). (PAICS PurC and PurC−PurE linker sequences were removed.) Similar phylogenetic trees were obtained for selected class II PurEs analyzed by ML (Figure 3) or NJ (Figure S1 of the Supporting Information) methods. *Td*PurE and *Af*PurE groups are part of the class II PurE clade. There is moderate support for a deep node containing *Af*PurE and *Td*PurE, which

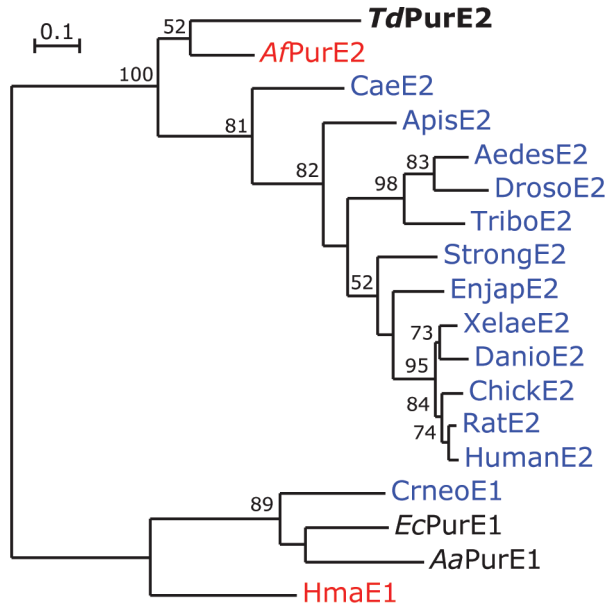

Figure 3. Evolutionary relationship among selected PurE sequences from bacteria (black), archaea (red), and eukarya (blue). The appended numeral (1 or 2) indicates a class I or class II PurE sequence. The four class I PurEs shown are three previously characterized forms and the most divergent form in class I alignments (HmaE1). A ClustalW alignment of 95 protein sequences was used to create a codon-aligned DNA alignment, of which 18 were analyzed using the ML method. The third nucleotide in each codon and all gap-containing positions were ignored. A bootstrap test of the inferred phylogeny was performed with 1000 replicates. The numbers at branches represent the percentage of replicate trees containing the indicated clustering (>50%). Branch lengths are proportional to evolutionary distances; the scale bar represents a distance of 0.1 substitution per site. Organism codes, taxonomic information, and sequence details are given in Tables S3−S9 of the Supporting Information.

are the only known class II PurEs not fused to PurC. They may derive from a primeval PurE that more closely resembled modern class II enzymes. The class I PurE clade was not well-resolved (Figure S1 of the Supporting Information), suggesting a complex evolutionary history. In some cases, PurEs from taxonomically unrelated organisms that occupy similar environmental niches appeared to cluster (e.g., AquiE1 and PaiE1, from the bacterium *Aquifex aeolicus* and the crenarchaeon *Pyrobaculum aerophilum*, respectively).

In contrast, PurK proteins and domains yielded well-resolved phylogenetic trees that were similar as determined by ML or NJ analysis (Figure S2 of the Supporting Information). The differences in phylogenetic tree structure and quality for these two closely linked enzymes suggest that PurK and PurE may have been subjected to different selective pressures.

***Td*PurE Purification and Characterization.** *Td*PurE is a 159-residue protein with a predicted pI of 7.7. *Td*PurE was expressed in *E. coli* using autoinduction medium and was readily purified using ammonium sulfate fractionation, followed by phenyl-Sepharose, hydroxyapatite, and gel filtration chromatography (Table 1). ESI-MS analysis was consistent with full-length *Td*PurE, including Met1 [17195 ± 3 Da (observed), 17195.8 Da (expected)]. A single peak was observed by gel filtration at 184 kDa [138 kDa (expected)]. The oblate PurE octamer probably accounts for the discrepancy. H40N-*Td*PurE isolated by the same method was also full-length [17174 ± 3 Da (observed), 17172.8 Da (expected)].

Table 1. Isolation of *Td*PurE

operation	protein (mg)	activity (units)	specific activity (s^{-1})[a]	yield (%)
streptomycin	712	3560	1.4	(28)
60% $(NH_4)_2SO_4$	112	12660	33	100
phenyl-Sepharose	66	9370	41	74
hydroxyapatite	51	6530	37	51
Superdex-200	25	4500	52	35

[a] Computed assuming one active site per 17189 Da subunit. One unit per milligram corresponds to a specific activity of 0.29 s^{-1}.

Steady-State Kinetics of *Td*PurE-Catalyzed Reactions. In the CAIR decarboxylase assay, *Td*PurE has a K_m of 9 μM and a k_{cat} of 65 s^{-1} at 30 °C and a K_m of 3.8 μM and a k_{cat} of 16 s^{-1} at 10 °C (assuming one active site per 17 kDa subunit). The value of k_{cat}/K_m increases by only 1.7-fold over this 20 °C interval. *Td*PurE is also more active than *Ec*PurE at both temperatures: 185 and 37 units mg^{-1} at 30 °C and 49 and 9.3 units mg^{-1} at 10 °C, respectively.

The specific activity of H40N-*Td*PurE in the CAIR decarboxylation assay (100 μM CAIR) was ~0.01 unit mg^{-1}, or 2×10^4-fold lower than that of wild-type *Td*PurE.[c] As with class I PurEs,[11,12] the universally conserved active site His (Figure 2) appears to be critical for activity.

Preliminary AIR carboxylation assays were performed under high-bicarbonate conditions (0.2 M) that either provide substantial CO_2 (class II PurE) or nonenzymatically convert some AIR to N^5-CAIR (class I PurE). These saturation curves gave an AIR k_{cat}/K_m of 6.4×10^3 M^{-1} s^{-1} (Figure S3 of the Supporting Information), which is 80-fold lower than the value reported for ChickE under similar conditions.[7] Inhibition was evident in CAIR decarboxylation assays performed under high-bicarbonate conditions, which gave a CAIR k_{cat}/K_m of 3.3×10^4 M^{-1} s^{-1}, some 220-fold lower than the value determined above. Higher activities were obtained using CO_2 as a substrate (described below).

pH Dependence of CAIR Decarboxylation. The CAIR decarboxylation reaction requires C4 protonation; the pH dependence of this reaction has not been reported for any class II PurE. A bell-shaped k_{cat}/K_m versus pH profile (Figure 4) was observed with a pK_1 of 5.7 ± 0.2 and a pK_2 of 7.3 ± 0.1. These findings are similar to results obtained with class I enzymes *Ec*PurE (pK_1 = 6.7, and pK_2 = 7.5)[12] and *Aa*PurE (pK_1 = 6.0, and pK_2 = 7.2),[11] as expected because all enzyme forms have the same ionizable enzyme groups and use the same CAIR substrate. The functional H59D-*Aa*PurE mutant was used to assign pK_2 to the active site His,[11] which is likely to play the same role in the class II PurE reaction.

The *Td*PurE k_{cat} versus pH profile was more complex, indicating a change in the kinetic mechanism at low pH (Figure 4). (Spontaneous CAIR decarboxylation, which increases at low pH,[5] was subtracted from the observed rates.) We considered the possibility that the *Td*PurE·CAIR Michaelis complex could form products by parallel pathways at low pH, with each contributing to the observed k_{cat}. This model and the derivation of eq 2, an expression for the pH dependence of the CAIR decarboxylation reaction, are given in Appendix 2 of the

Table 2. Crystallographic Data Collection and Refinement Statistics[a]

	*Td*PurE (PDB entry 3rg8)	*Td*PurE·AIR (PDB entry 3rgg)
	Data Collection	
space group	$P2_1$	$C222_1$
cell dimensions	a = 83.5 Å, b = 87.9 Å, c = 86.7 Å	a = 84.4 Å, b = 155.1 Å, c = 88.1 Å
	$\alpha = \gamma = 90°$, $\beta = 118.3°$	$\alpha = \beta = \gamma = 90°$
resolution (Å)	19.6−1.74 (1.79−1.74)	37.1−1.82 (1.87−1.82)
no. of reflections (total)	410467 (29077)	325864 (18126)
no. of reflections (unique)	112698 (8305)	51257 (3520)
redundancy	3.6 (3.5)	6.3 (5.1)
completeness (%)	99.5 (99.5)	98.6 (92.3)
R_{sym}[b] (%)	5.1 (59.1)	6.4 (86.5)
$\langle I/\sigma \rangle$	17.5 (2.1)	20.0 (2.2)
	Refinement	
resolution (Å)	19.6−1.74 (1.77−1.74)	37.1−1.82 (1.87−1.82)
no. of reflections	106915 (5694)	48510 (3510)
completeness (%)	97.2 (82.9)	98.3 (92.1)
R_{cryst}[c] (%)	16.5 (20.1)	18.6 (38.0)
R_{free}[d] (%)	20.0 (29.3)	21.7 (40.7)
twin fraction (initial/final)	0.23/0.359	—
twin law	$(-h,-k,h+l)$	—
no. of protein atoms	9496	4708
no. of ligand atoms	—	76
no. of buffer atoms	8	—
no. of water atoms	825	292
rmsd		
bond lengths (Å)	0.016	0.016
bond angles (deg)	1.547	1.682
average B factor (Å^2)		
protein atoms	22.3	35.7
ligand atoms	29.4	37.5
water atoms	25.0	36.1

[a] Values in parenthesis are for the highest-resolution shell. [b] $R_{sym} = \Sigma|I_h - \langle I_h \rangle|/\Sigma I_h$, where $\langle I_h \rangle$ is the average intensity over symmetry. [c] $R_{cryst} = \Sigma||F_o| - \langle |F_c| \rangle|/\Sigma|F_o|$, where the summation is over the data used for refinement. [d] R_{free} is defined in the same way as R_{cryst} but was calculated using the 5% of the data that were excluded from the refinement.

Supporting Information. A fit of the data to eq 2 gave a pK_1 of 5.9 ± 0.5 and a pK_2 of 8.4 ± 0.1. These pK_a values are similar to those for class I enzymes *Ec*PurE (pK_1 = 5.9, and pK_2 = 8.6)[12] and *Aa*PurE (pK_1 = 5.1, and pK_2 = 8.4).[11] However, in class I PurEs, pK_1 is associated with suppression of activity, due to protonation of CAIR N3 within the Michaelis complex,[11] whereas class II PurE shows activation of activity (Figure 4).

N^5-CAIR Regeneration System. Ultraviolet absorbance spectroscopy is routinely used to monitor the conversion of CAIR to AIR and N^5-CAIR, each of which has an extinction coefficient lower than the extinction coefficient of CAIR. Both PurE classes are expected to form the same equilibrium product distribution containing mainly AIR, because of the spontaneous decarboxylation of N^5-CAIR. To assess its ability to function as a PurE substrate, it is desirable to maintain the N^5-CAIR concentration at a high steady-state level. This can be achieved at low bicarbonate concentrations using *Ec*PurK- and ATP-dependent resynthesis.[4] However, the high level of ATP required is incompatible with quantitation by absorbance of aminoimidazole mononucleotides.

We developed an ATP/N^5-CAIR regenerating system that allowed for spectrophotometric monitoring of PurE reaction mixtures at low ATP levels (Appendix 3 of the Supporting Information). A central concern was to minimize the spectral contribution of reaction mixture components in the ultraviolet region of interest. ATP regeneration by pyruvate kinase and phosphoenolpyruvate fails with respect to this criterion. Next, we considered acetate kinase and acetyl phosphate, which have no significant absorbance in the 230−300 nm range at the required concentrations. Unfortunately, this system does not support recycling of N^5-CAIR (data not shown). We speculate that PurK is inhibited by acetyl phosphate, which resembles the carboxyphosphate reaction intermediate.[52]

We resorted to creatine phosphate/creatine kinase (CrP/CK), which has no absorbance in the 242−300 nm range and is known to support PurK activity.[22] The CK reaction has a weaker preference for ATP regeneration (10−20-fold[53−55]) than the aforementioned ATP regeneration systems.[56] The irreversibility of the PurK reaction, as judged by its inability to convert ADP, P_i, and N^5-CAIR into ATP and AIR,[57] further ensures efficient recycling. We found 50 μM ATP to be an acceptable compromise between background absorbance and efficient N^5-CAIR regeneration, even though this level is both

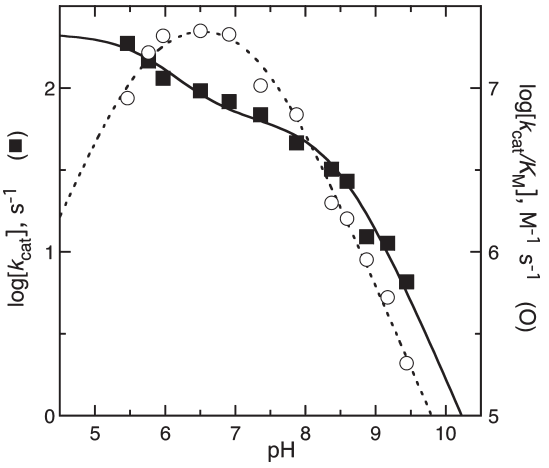

Figure 4. pH dependence of the CAIR decarboxylase reaction. The k_{cat}/K_m data (right ordinate, ○) fit to eq 1 with a $\tilde{k}_{cat}/\tilde{K}_m$ of (2.9 ± 0.5) × 10^7 M^{-1} s^{-1} (···). The k_{cat} data (left ordinate, ■) fit to eq 2 with a $\tilde{k}_1$ of 210 ± 70 s^{-1} and a $\tilde{k}_2$ of 63 ± 9 s^{-1} (—). The two pK_a values obtained in each fit are given in the text.

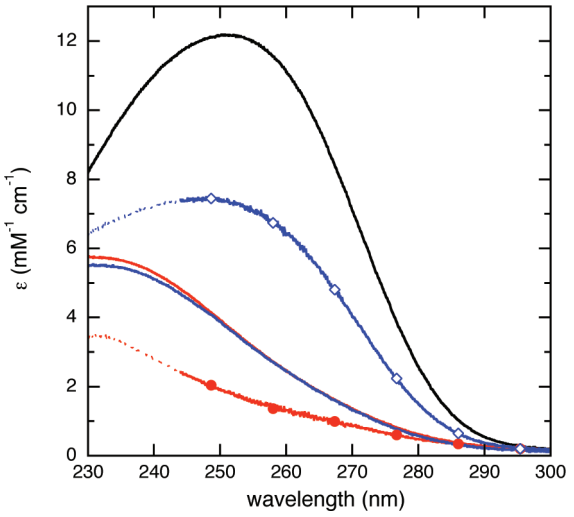

Figure 5. Divergent products formed from CAIR by different PurEs in the presence of *Ec*PurK at steady state. CAIR (black trace) is converted to an equilibrium distribution of mononucleotides (AIR, N^5-CAIR, and CAIR) by the addition of either *Ec*PurE (blue trace without symbols) or *Td*PurE (red trace without symbols). The addition of *Ec*PurK to the *Ec*PurE reaction mixture leads to an increase in absorbance due to CAIR formation (blue trace with diamonds). In contrast, the addition of *Ec*PurK to the *Td*PurE reaction mixture leads to a further decrease in absorbance due to depletion of CAIR (red trace with circles). The latter spectrum is similar to that of N^5-CAIR alone, indicating it is not a substrate for *Td*PurE. In these experiments, the decomposition of N^5-CAIR has been minimized by the addition of bicarbonate. All PurK reaction mixtures also contain ATP, CK, and CrP (Appendix 3 of the Supporting Information). While contributions due to enzyme(s) and buffer components have been subtracted, some change due to the conversion of CrP to Cr is expected at lower wavelengths; absorbance spectra containing the N^5-CAIR recycling system are depicted as dotted lines below 244 nm. A control reaction without PurE shows no significant difference in the CAIR spectrum after the addition of *Ec*PurK (data not shown). The extinction coefficients given are higher than reported values.[2,6,57] This appears to be an unsubtracted background component derived from slow AIR decomposition. The observed $\Delta\varepsilon_{260}$ of 9.79 mM^{-1} cm^{-1} between the CAIR spectrum (black trace) and the *Ec*PurK/*Td*PurE spectrum (thick red trace) is exactly the same as the difference between published ε_{260} values for CAIR (10.50 mM^{-1} cm^{-1}) and N^5-CAIR (0.71 mM^{-1} cm^{-1}). This provides additional evidence that the most abundant mononucleotide present in the *Ec*PurK/*Td*PurE reaction mixture is N^5-CAIR.

subsaturating for *Ec*PurK (K_m = 90 μM)[6] and comparable to the aminoimidazole mononucleotide concentrations present.

The conversion of AIR to N^5-CAIR in the presence of CrP/CK shows a decrease in absorbance below 244 nm due to CrP consumption (Figure S9 of the Supporting Information). This spectral region was excluded from aminoimidazole analysis. Difference spectra also exhibit a small increase at 250−260 nm, which is probably due to slow, nonenzymatic formation of CAIR. The distribution of aminoimidazole mononucleotides is not significantly affected by this phenomenon.

At pH 8, the K_{eq} for the *Ec*PurE reaction measured by this method is ∼1.2, favoring CAIR slightly (data not shown). This is in reasonable agreement with a K_{eq} of 1.8 at pH 7.8 reported for the *Ec*PurE-mediated and nonenzymatic equilibration of "AIR" (likely a mixture of AIR and N^5-CAIR) and CAIR.[6] The class II reaction is expected to be much less favorable at neutral pH and low CO_2 levels. Parallel experiments performed with *Td*PurE in the absence of the ATP regenerating system indicate that [AIR]/[CAIR] ∼ 7 at 1 mM CO_2 and pH 8 (data not shown).

N^5-CAIR Is Not a *Td*PurE Substrate. All PurEs are thought to form ternary PurE·AIR·CO_2 complexes, which means that an "ambidextrous" PurE form with both class I and class II activities (that is, one that can use N^5-CAIR and AIR/CO_2) may exist. As a deeply branched form, *Td*PurE is a logical candidate. Here we examined its ability to use N^5-CAIR as a substrate. N^5-CAIR has not previously been excluded as a class II PurE substrate, because it forms spontaneously under the high-bicarbonate/CO_2 conditions typically used for AIR carboxylase assays.

The addition of either *Td*PurE or *Ec*PurE to a solution of CAIR results in similar ultraviolet spectra (Figure 5) that resemble the AIR spectrum.[6] AIR is the predominant species present in each reaction mixture because of direct, enzyme-mediated formation of AIR (*Td*PurE) or spontaneous decarboxylation of N^5-CAIR (*Ec*PurE).

The reaction outcomes diverge sharply when *Ec*PurK is added to each PurE reaction mixture. The addition of *Ec*PurK to *Ec*PurE reaction mixtures results in an increased absorbance, indicating that N^5-CAIR is converted to CAIR; the steady-state concentrations of N^5-CAIR and CAIR are comparable. In contrast, the addition of *Ec*PurK to *Td*PurE reaction mixtures results in a decreased absorbance similar to that in a spectrum of N^5-CAIR recorded at pH 7.8 and 4 °C.[57] This demonstrates that *Td*PurE cannot convert N^5-CAIR to CAIR, as expected for a dedicated class II PurE.

CO_2 Is a *Td*PurE Substrate. High bicarbonate levels can often provide sufficient CO_2 to support class II PurE reactions.[7] However, preliminary steady-state experiments (Figure S3 of the Supporting Information) showed unexpectedly low activities, possibly due to inhibition by bicarbonate or N^5-CAIR, which would be present at high levels in this assay.[7] CO_2 can also be provided from a saturated aqueous solution, providing substrate until it is depleted by $CO_2 \rightleftharpoons HCO_3^-$ equilibration.[1] Controls showed that relatively little bicarbonate is initially present: for a predicted delivery of 0.48−29 mM CO_2, we measured $[CO_2]_T$ values of 0.5−30 mM in equilibrated reaction mixtures. Conditions were chosen such that CO_2 equilibration ($t_{1/2}$ ∼ 90 s)[1,58] is

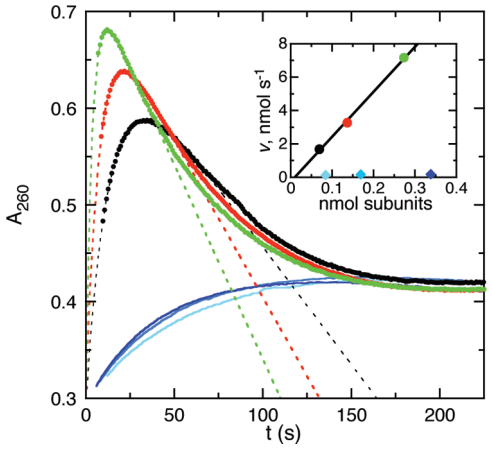

Figure 6. Formation of CAIR upon addition of CO_2 to solutions containing PurE and AIR. At time zero, CO_2 was added from a saturated stock (final concentration of 20 mM) to a solution containing 0.1 mM AIR and varying amounts of PurE at 10 °C and pH 8. The solid lines illustrate progress curves for solutions containing *Ec*PurE (0.84−3.3 nmol of subunits, from light to dark blue; 0.14−0.56 unit in the CAIR decarboxylation assay at 10 °C). The symbols illustrate progress curves for *Td*PurE at 0.068 nmol of subunits (0.058 unit) (black symbols), 0.14 nmol of subunits (0.12 unit) (red symbols), or 0.27 nmol of subunits (0.23 units) (green symbols). Dotted lines indicate fits of the initial ~50 s for the *Td*PurE progress curves to eq 3, which are used to obtain initial velocities with eq 5. The missing time points at the beginning of each trace represent the time required to add CO_2, mix the solution, and replace the cuvette. Mechanical mixing methods were not used because the CO_2 solution is bubbled until the last possible moment. The inset shows the enzyme concentration dependence of the initial velocity (color-coded as in the main panel). Note that the *Ec*PurE concentrations indicated on the abscissa have been divided by 10.

slower than class II PurE-mediated conversion of AIR and CO_2 to CAIR.

Both *Td*PurE and *Ec*PurE reaction mixtures showed an initial increase at A_{260} due to CAIR formation (Figure 6), which is enzyme-catalyzed (class II PurE) or due to the eventual conversion of nonenzymatically formed N^5-CAIR to CAIR (class I PurE). The initial formation of CAIR is much faster in *Td*PurE reaction mixtures than in those containing *Ec*PurE. The subsequent decrease in absorbance after a few minutes can be explained by the conversion of CO_2 to HCO_3^- as the CO_2−HCO_3^- equilibrium is established. *Td*PurE increasingly favors CAIR decarboxylation as the CO_2 concentration decreases. The kinetic complexity of the back-reaction period precludes a detailed simulation of the whole progress curve. However, the initial absorbance decrease corresponding to the back-reaction was adequately represented by a simple line (eq 3). This allowed fitting of the first ~55 s of the time course (dotted lines in Figure 6) and estimation of initial CAIR formation velocities (eq 5).

The initial velocity of formation of CAIR by *Td*PurE was linearly dependent on enzyme concentration (inset of Figure 6), with a slope corresponding to a k_{cat} of 27 s^{-1}. In contrast, initial velocities in the *Ec*PurE reactions showed no dependence on enzyme concentration (average value of 0.2 nmol s^{-1} in this experiment) even in the presence of large amounts of the class I PurE. The slow increase in the *Ec*PurE reaction mixtures is likely due to nonenzymatic formation of N^5-CAIR, which is slower than either the subsequent *Ec*PurE-mediated conversion of N^5-CAIR to CAIR or CO_2-dependent, *Td*PurE-mediated CAIR formation. As anticipated, reaction mixtures containing either PurE approached a comparable, increased absorbance value after a few minutes, indicating a similar equilibrium distribution of aminoimidazole mononucleotides that undergoes an increase in CAIR concentration due to the increase in $[CO_2]_T$.

The CO_2-dependent activity assay allowed the determination of kinetic constants for the *Td*PurE-mediated AIR carboxylation reaction (Figure S4 and Table S10 of the Supporting Information). The K_m value at 10 °C for CO_2 was 13 mM at saturating levels of AIR. The corresponding value for ChickE at 37 °C was determined using a $KHCO_3$-dependent assay (23 mM $KHCO_3$ or <0.8 mM CO_2).[7] The k_{cat} values are comparable: 77 s^{-1} for *Td*PurE and 32 s^{-1} for ChickE.

The K_m value for AIR was ~60 μM at near-saturating levels of CO_2. The *Td*PurE $k_{cat}/K_m = 1 \times 10^6$ M^{-1} s^{-1} (AIR) at 10 °C. The comparable value for ChickE is 5×10^5 M^{-1} s^{-1}.[7]

Crystallographic Characterization of *Td*PurE. The crystal structure of *Td*PurE was determined by molecular replacement (Table 2). *Td*PurE has the same protein fold as class I PurE[9] and the class II PurE domain of PAICS.[13] The eight monomers of *Td*PurE resemble each other closely, differing only in the conformations of residues at the N- and C-termini. The *Td*PurE monomer aligns with *Ec*PurE (PDB entry 1qcz) with a root-mean-square deviation (rmsd) of 1.24 Å over 145 Cα atoms and with *Aa*PurE (PDB entry 2fwj) with an rmsd of 1.15 Å over 140 Cα atoms. It aligns with the PurE domain of human PAICS (PDB entry 2h31) with an rmsd of 0.93 Å over 152 Cα atoms.

Class I and class II PurE sequences are distinguished by differentially conserved residues, i.e., those that are highly conserved but are different in each class (Figure 2). Three such differences map to the active site "70s loop" (Figure 7D). First, a His (*Ec*PurE His75 and *Aa*PurE His89) is replaced with a smaller residue (*Td*PurE Ala71 and PAICS Gly334). Second, a small residue (*Ec*PurE Gly72 and *Aa*PurE Gly86) is replaced with an Arg (*Td*PurE Arg68 and PAICS Arg331). The methylene groups of Arg68 form part of the active site, but the guanidinium moiety extends to the surface, where Nω contacts the backbone carbonyl of conserved residue Met105′ [Met105 from a neighboring monomer (Figure 7B)]. Third, an Ala (*Ec*PurE Ala74 and *Aa*PurE Ala88) is replaced with *Td*PurE Asn70. [The replacement of a nearby Pro (*Ec*PurE Pro77 and *Aa*PurE Pro91) with a smaller residue (*Td*PurE Ser73 and PAICS Gly336) appears to sterically accommodate Asn70.] The side chain of Asn70 makes a capping interaction at the end of helix α3, interacting with Ser73 NH and Oγ, and also Leu72 NH. Another contact is made with Ser102 in helix α4, an absolutely conserved, class II-specific residue. The side chain of PAICS Asn333 makes comparable interactions with the helix backbone, but the only side chain−side chain interactions are with Ser349 and Ser365 (the equivalent of *Td*PurE Ser102). This substructure appears to increase the rigidity of the class II PurE 70s loop relative to that in class I PurEs, which makes no side chain−backbone interactions.

The crystal structure of *Td*PurE bound to AIR was obtained using data from a *Td*PurE crystal that had been soaked with CAIR (Table 2). The *Td*PurE·AIR complex crystallized in space group $C222_1$, with half of the octamer represented in the asymmetric unit. The N-terminus of chain D was modeled as a carbamate that contacts the Ser91 hydroxyl group and the Asp92 amide nitrogen in an adjacent octamer. We hypothesize that this adduct is formed from bicarbonate provided by the CAIR solution. (No ESI-MS peak consistent with N-formylated Met1 was observed.)

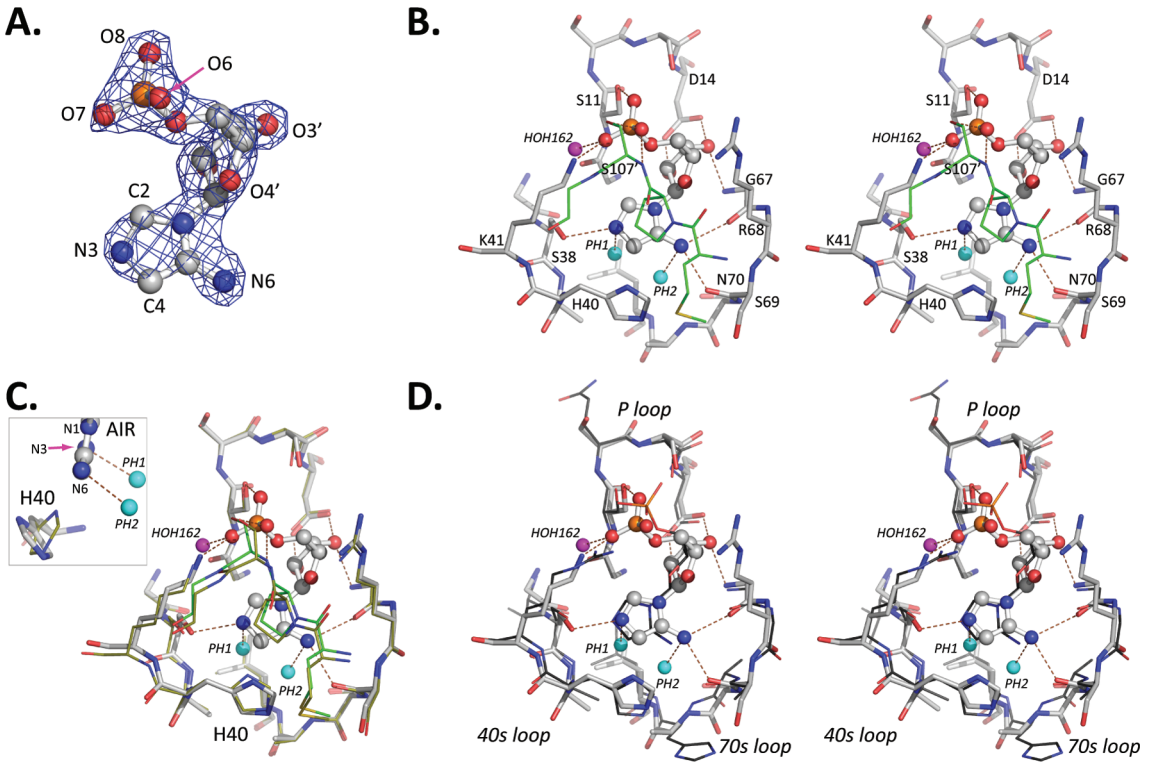

Figure 7. PurE·AIR complexes. (A) View of the ligand in the refined *Td*PurE·AIR model superimposed onto the $2F_o - F_c$ electron density map (contoured at 1.5σ; PDB entry 3rgg). (B) Stereodiagram of the *Td*PurE·AIR complex (PDB entry 3rgg) with ligand-contacting residues labeled. Panels B–D present the same orientation of the active site (stick rendering, gray carbon atoms) and ligands (ball-and-stick rendering). The segment containing Ser107′ is shown in thin stick rendering with green carbon atoms. Placeholder waters (PH1, HOH160; PH2, HOH161) and the portal water (HOH162) are shown as cyan or magenta spheres. (C) Comparison of *Td*PurE (thin stick rendering, with dark green carbon atoms, PDB entry 3rg8) with the *Td*PurE·AIR complex. In the inset, a perpendicular view from the right demonstrates the His40 ring rotation. (D) Stereodiagram superposing the *Aa*PurE·AIR complex (black carbon atoms, PDB entry 2fwj) onto the *Td*PurE·AIR complex. Both crystals were grown at pH 8.0 and soaked with CAIR prior to being flash-cooled and prior to data being collected.

The enzymatic product AIR was built into clear electron density (Figure 7A) in all active sites. AIR adopts four slightly different conformations; only the AIR in subunit A is discussed here (Figure 7B). Several polar interactions are typical for PurE bound to aminoimidazole mononucleotides: the Ser11 hydroxyl group contacts phosphate O8, Asp14 contacts both ribose hydroxyls, and the Ser38 hydroxyl group contacts aminoimidazole N3.

The *Td*PurE active site is mostly preorganized to bind AIR (Figure 7C). The first difference is a shift in the position of Ser107′, in which the hydroxyl group swivels ~110° to form a hydrogen bond with AIR phosphate O6. This is the first example of a polar contact between a bound mononucleotide and an adjacent PurE subunit. (Ser107 is conserved in class II PurE only.) The second difference is an ~70° rotation of the His40 side chain, about an axis passing through Cβ and Nε2, that avoids a clash with AIR C4.

Similar solution conditions were used to prepare AIR complexes for *Aa*PurE[11] and *Td*PurE to allow a close comparison of class-specific interactions. AIR is a competitive inhibitor of class I PurEs[2,57] but is a substrate for class II PurEs. The AIR conformations in these complexes differ most in the position of the phosphate moiety (Figure 7D). The interaction with the differentially conserved residue *Td*PurE Lys41, which is shorter than the corresponding class I Arg, appears to pull the AIR deeper into the active site pocket. *Aa*PurE Arg60 forms hydrogen bonds with two phosphate oxygens. In *Td*PurE, this role is performed by Lys41, which forms a hydrogen bond with only one phosphate oxygen, and Ser107′ (Gly126′ in *Aa*PurE), which contacts a different phosphate oxygen.

The aminoimidazole moiety is closer to the 70s loop in the *Td*PurE·AIR complex than in the *Aa*PurE·AIR complex (Figure 7D). In the *Td*PurE·AIR (substrate) complex, AIR exocyclic amine N6 contacts two backbone carbonyl oxygens (Gly67, 3.1 Å; Ser69, 2.8 Å) in the differentially conserved 70s loop, whereas the corresponding *Aa*PurE·AIR (inhibitor) and dead-end H59N-*Aa*PurE·AIR·CO_2 complexes show only one contact (Figure S5 of the Supporting Information). This region is located near the amino-terminal (positive-dipole) end of helix α2.

Additional steric constraints are provided by *Td*PurE Arg68, which is sandwiched between AIR (C4′ and C5′) and Arg104′. In turn, Arg104′ appears to be held in place by a salt bridge with the universally conserved residue Asp98 and differentially conserved residues in surrounding loops. Class I PurEs do not have these contacts: Gly72 and Gln109 of *Aa*PurE and Arg68 and Arg104 of *Td*PurE are differentially conserved residues.[d] As described above, the conformation of the class II 70s loop appears to be buttressed by the Asn70–α3 helix-capping interaction, which is not found in the comparatively flexible, Ala- and Gly-rich class I 70s loop.

As described above, the *Td*PurE His40 imidazole rotates upon AIR binding. The corresponding *Aa*PurE His59 imidazole does

not. In both complexes, His Nδ is on the *re* face of the aminoimidazole (Figure 7D). In the *Aa*PurE·AIR complex, the His59 imidazole and AIR aminoimidazole rings are oriented in near-parallel planes, with a His Nδ−AIR C4 separation of 3.5 Å. In the *Td*PurE·AIR complex, these planes form an ∼55° angle and the Nδ−C4 separation is 3.7 Å.

Carboxylate/CO_2 Binding Site. Class I PurE active sites contain a carboxylate/CO_2 binding subsite that is variously occupied by nucleotide carboxylates, CO_2, the NO_2 group in the competitive inhibitor 4-nitro-AIR, or two well-ordered and highly conserved waters ("placeholder waters").[12] Quantitative retention of CO_2 formed transiently by class I PurE has been demonstrated.[8]

Placeholder waters are present in both *Td*PurE structures (Figure 7C). Placeholder water 1 (HOH160) interacts with the amide NH group of Ala39 (in *Aa*PurE, HOH688 and Ala58; PDB entry 1u11). Placeholder water 2 (HOH161) interacts with the amide NH groups of Ala71 and Leu72 (in *Aa*PurE, HOH691 and His89/Leu90). The placeholder waters are ∼2.7 Å apart; analogous O−O separations are 2.31 Å in CO_2 and 2.21 Å in CAIR (in the H45N-*Ec*PurE·CAIR complex, PDB entry 2nsl).[12] An atom located halfway between the placeholder waters would be well-placed to react with AIR C4, 2.4 Å away. The catalytically arrested mutant H59N-*Aa*PurE·AIR·CO_2 complex (PDB entry 2fwp)[e] has an AIR C4−CO_2 carbon−carbon distance of 2.7 Å.[11,12]

The absence of a bulky side chain at *Td*PurE Ala71 (analogous to *Ec*PurE His75) creates a "remote pocket" outside the active site that is occupied by two well-ordered water molecules. In the PAICS structure, the remote pocket contained electron density in the $F_o - F_c$ map that was reported to correspond to a CO_2 molecule bound on a 2-fold crystallographic axis.[13] This location is not consistent with the required covalent interaction between CO_2 and AIR C4, which would be separated by ∼7.8 Å, nor is it clear how CO_2 would access this site. We recalculated the $F_o - F_c$ electron density map using the PAICS model with CO_2 removed and found that the CO_2 density was difficult to discern from background noise. We then calculated a σA-weighted $2F_o - F_c$ electron density map using the PAICS model with the CO_2 occupancy corrected as described in Experimental Procedures; this map had almost no electron density at the position of the modeled CO_2. Given the weak electron density and the relatively low resolution of the crystal structure, the evidence of CO_2 binding in the remote pocket of PAICS is not compelling.

A Possible Portal for CO_2. In contrast to the tight retention of transiently formed CO_2 by class I PurE, class II PurEs must allow the binary PurE·AIR complex to bind or to dissociate from CO_2. The *Td*PurE·AIR complex appears to contain a portal for CO_2 that leads to the carboxylate/CO_2 binding site, the deepest part of the active site (Figure 8D). The narrowest constriction is defined by the Cα atom and backbone oxygen of Gly10, the Cβ atom of Ser38, and the C2 atom of the AIR aminoimidazole ring. In most subunits, a "portal water" (HOH162), located just outside this constriction, is 6.3 Å from the CO_2 binding site, defined by placeholder water 1 (HOH160) (Figure 7B). The portal water also makes polar contacts with an AIR phosphate oxygen (O7), Nε of the class II-specific residue Lys41, the backbone oxygen of Gly10, and several external waters that are in contact with bulk solvent. Contacts with Ser38 appear to stabilize the constriction, including several polar interactions between its hydroxyl group and the backbone amides of His40 and Lys41, and with N3 of the AIR aminoimidazole ring. A CO_2 entering the active site along the path from the portal water to placeholder water 1 would pass alongside AIR phosphate O7 and then aminoimidazole ring C2, both of which are opposite AIR exocyclic amine N6. AIR C2 is farther from from the portal residue *Td*PurE Gly10 than it is from the corresponding class I residue (*Aa*PurE Gly29).

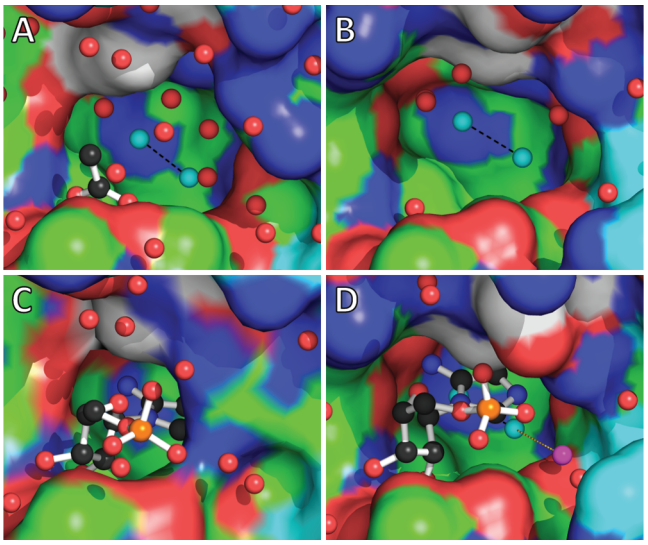

Figure 8. Surface rendering of *Aa*PurE (A and C) or *Td*PurE (B and D), in the absence (A and B) or presence (C and D) of AIR. All crystal structures were superimposed using backbone atoms of subunit A and are shown from the same orientation outside the putative CO_2 portal. The placeholder waters (cyan spheres connected by black dotted line) indicate the CO_2 binding site at the bottom of the active site pocket. The gold dotted line in panel D is the shortest path (6.3 Å) from the portal water (magenta sphere, HOH162) to placeholder water 1 (HOH160) and may represent the path by which CO_2 enters the *Td*PurE·AIR binary complex. Note that a similar path is not present in the *Aa*PurE·AIR complex (C); class I PurE traps transiently formed CO_2.[8] Surfaces are colored by element (red, oxygen; blue, nitrogen) or chain (protein carbon atoms colored green in subunit A, cyan in subunit B, and white in subunit F). Crystals were grown and soaked at pH 8.0, except for *Aa*PurE (PDB entry 2fw1) in panel A, which was crystallized at pH 8.5 and contains an adventitiously bound acetate. An alternate view of panel D is presented as a stereodiagram in Figure S6 of the Supporting Information.

DISCUSSION

Physiological Consequences of PurE Class Selection. *Td*PurE is the only bacterial class II *purE* sequence currently known. Despite clear sequence differences (Figure 3), *Td*PurE contains all class-specific, differentially conserved residues and is functionally and structurally similar to ChickE[5,7] and HumanE.[13] The similar sequences of bacterial *Td*PurE and archaeal *Af*PurE suggest both an ancient origin for class II PurEs and the possibility that *T. denticola* did not acquire its unusual PurE from an animal host.

Environmental factors like ambient CO_2 concentration may dictate the selection of a particular PurE class.[8] Some microbes that contain a class I PurE, but lack PurK, appear to rely upon the spontaneous formation of N^5-CAIR from AIR at elevated CO_2 levels (Table S7 of the Supporting Information). This seems less efficient than the direct use of AIR and CO_2 by the class II PurE in *T. denticola*; perhaps the class II PurE equilibrium, disfavoring

CAIR formation, is a limitation. CO_2 availability should be particularly important for purine biosynthesis in *T. denticola*.

Cytoplasmic CO_2−bicarbonate equilibration may be a significant influence on PurE class selection. Carbonic anhydrase is essential under low-CO_2 conditions in many bacteria and yeasts, including some pathogens.[59,60] Decarboxylase enzymes produce CO_2 as a product, whereas carboxylase enzymes generally consume bicarbonate and ATP. The essential function of carbonic anhydrase has been proposed to be capturing metabolically produced CO_2 as the membrane-impermeant bicarbonate, for use in fatty acid, amino acid, and nucleotide biosynthesis.[61] Under low-CO_2 conditions in the absence of carbonic anhydrase, the spontaneous conversion of CO_2 to bicarbonate could be a growth-limiting factor.

Carbonic anhydrase has not been detected in any spirochete or in *A. fulgidus*.[62] The direct use of CO_2 in purine biosynthesis may therefore be advantageous to *T. denticola*, by lowering biosynthetic bicarbonate demand relative to the demands of other bacteria. Furthermore, CO_2 is more readily available in the anaerobic niches occupied by *T. denticola* and *A. fulgidus*, as it was in the anoxic Archaean atmosphere.[63,64]

Structural Divergence of PurE Classes: N^5-CAIR and CO_2 Binding. Only class I PurE performs the N^5-CAIR → AIR·CO_2 half-reaction (Figure 1).[12] Structural reasons for this functional difference are not apparent in a comparison of unliganded PurE structures.[13]

While N^5-CAIR is not a *Td*PurE substrate, it could be an inhibitor that forms spontaneously in high-CO_2 environments. The AIR binding mode may disfavor N^5-CAIR binding or formation by *Td*PurE. A superposition of N^5-CAIR from the *Ec*PurE·N^5-CAIR complex (a revision of PDB entry 1d7a)[9,12] onto ligand atoms in the *Td*PurE·AIR complex would cause the carbamate oxygens to clash with the side chains of universally conserved residues Ala66 and Leu72 of *Td*PurE.

Aminoimidazole ring flipping in class I PurE complexes may determine whether C4 (leading to CAIR) or N6 (leading to N^5-CAIR) reacts with the sequestered and immobilized CO_2.[12] Comparisons with the dead-end ternary complex, H59N-*Aa*PurE·AIR·CO_2, indicate that less motion is required for the AIR·CO_2 → CAIR conversion (class I and class II) than for the N^5-CAIR → AIR·CO_2 conversion (class I-specific). This difference may explain why the class I active site appears to be less rigid than the class II active site.

Class I and II PurEs differ starkly in their respective requirements for preventing or allowing CO_2 association and/or dissociation. Class I PurE·AIR·CO_2 intermediate complexes must effectively prevent CO_2 escape, which equates to a waste of ATP by PurK.[8,9,11] In contrast, class II PurE·AIR complexes must effectively trap CO_2 that reaches the bottom of the active site, possibly by increasing the reactivity of AIR C4.

The binary *Td*PurE·AIR structure shows how CO_2 might enter its binding pocket below AIR, but after AIR binding: a CO_2 portal allows access to the bottom of the active site (Figure 8). In contrast, class I PurE lacks a portal and is competitively inhibited by AIR,[57] which cannot form a productive ternary complex. The differentially conserved residue Lys41 (and Ser107′) reorients the AIR phosphate to create the portal, an important class-specific role.

The *Td*PurE His40 ring rotation is the most obvious class-specific difference upon AIR binding. Another is the stronger interaction of AIR with the *Td*PurE 70s loop carbonyl oxygens, which would increase the electron density at C4. This should increase the likelihood that CO_2 entering the active site will form isoCAIR. In class I PurE, the electron density at C4 may also be modulated by variable interactions with the 70s loop. The dead-end ternary H59N-*Aa*PurE·AIR·CO_2 complex (PDB entry 2fwp) shows a unique backbone rotation that moves the Ala87 carbonyl away from the AIR exocyclic amine (Figure S5 of the Supporting Information).

Functional Divergence of PurE Classes: pH−Rate Profiles. Unlike the class I PurE reaction (Figure 1), the class II PurE equilibrium involves a proton; low pH favors CAIR decarboxylation. In the CAIR decarboxylase reaction, the two PurE classes diverge only after CAIR C4 protonation and decarboxylation to form a ternary PurE·AIR·CO_2 complex.[8,12] Class II PurE dissociates AIR and CO_2 and absorbs a proton to reset for the next cycle (Figure 9). Class I PurE continues with the half-reaction that forms N^5-CAIR by nucleophilic attack on the sequestered CO_2.

Class I PurE and *Td*PurE CAIR decarboxylase k_{cat}/K_m values have bell-shaped pH profiles with similar pK_a values (Figure 4), indicating that comparable ionizations occur in the free enzyme (or CAIR). Our assignment of pK_2 to deprotonation of the critical His residue and our suggestion that pK_1 corresponds to CAIR N3 protonation[11] also appear to be plausible for *Td*PurE. However, the shapes of the pH−k_{cat} profiles are strikingly different, indicating that pK_1 has a different kinetic consequence in the enzyme−substrate complex formed by each PurE class.

Protonation at N3 or C4 is required for nonenzymatic decarboxylation of CAIR or its analogues.[65] In solution, protonation at N3 has pK_a values of 6.05 and 5.9 for the nucleoside analogues of AIR and CAIR, respectively.[66] In the class I PurE working mechanism (Figure 1), N3 protonation is electrostatically incompatible with subsequent C4 protonation.[11,12] Class I PurEs appear to redirect protonation to the adjacent C4 atom to form isoCAIR, perhaps with the assistance of a universally conserved 40s loop Ser functioning as a hydrogen bond donor[11,12] (left series, Figure 9). Decarboxylation of isoCAIR would then furnish the key AIR·CO_2 intermediate. In the absence of the general acid (His59), N3 protonation might have a role in forming the dead-end H59N-*Aa*PurE·AIR·CO_2 complex.[12]

Our tentative model for the *Td*PurE k_{cat} increase corresponding to pK_1 also involves CAIR N3 protonation (right series, Figure 9). Here *Td*PurE Ser38 facilitates CAIR N3 protonation by functioning as a hydrogen bond acceptor. The timing of C4 protonation and decarboxylation may be reversed if N3 is protonated. Initial C4 protonation (forming isoCAIR-H$^+$, a ring with two positive charges) would be associated with prohibitive electrostatic barriers, as previously discussed.[11] Alternatively, initial decarboxylation could form the nitrogen ylide of AIR (yAIR), a proposed intermediate in CAIR ribonucleoside decarboxylation.[65] The negative charge at C4 would be stabilized by interactions with the polarized CO_2 carbon, protonated His40, and protonated N3 (box in Figure 9). Similar intermediates have been proposed for 3-aminopicolinic acid decarboxylation[67] and for orotidine 5′-monophosphate decarboxylase.[68] However, the yAIR mechanism has been criticized[69] because N3 in the class II-selective inhibitor 4-nitro-AIR[70] is difficult to protonate.[71] A concerted C4 protonation−decarboxylation reaction might skirt implausible stepwise reaction intermediates.

The finding that H40N-*Td*PurE is inactive is consistent with a required interaction between CAIR and His40. The imidazole tilt observed here may allow protonated His40 to interact differently

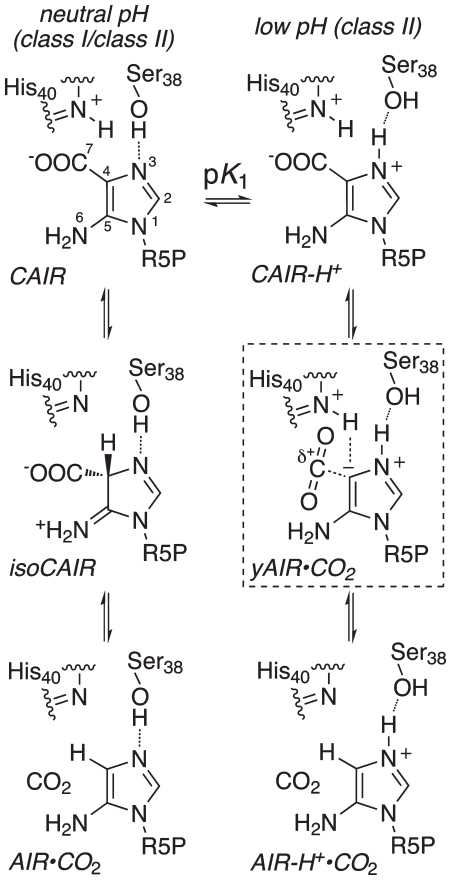

Figure 9. Working hypothesis for the mechanism of *Td*PurE, drawn in the CAIR → AIR direction. The numbered CAIR molecule is the presumptive major species at neutral pH. This depiction highlights the essential role of His40 (the likely origin of pK_2 for both PurE classes). The left-hand sequence is the full class II reaction and is analogous to the first half-reaction performed by class I PurEs. (In class I PurEs, the CO_2 is retained for the synthesis of N^5-CAIR in a second half-reaction that is not shown.) In the right-hand sequence, pK_1 corresponds to AIR N3 protonation and reversal of the polarity of the N3−Ser38 hydrogen bond. The k_{cat} acidic-arm pK_1 values for class I *Aa*PurE and *Ec*PurE (5.1 and 5.9, respectively) are comparable to that for *Td*PurE (5.7) and the CAIR N3 pK_a. The AIR nitrogen ylide (yAIR, box) is one possible intermediate in the low-pH series. Concerted protonation and decarboxylation is also a possibility.

with CAIR than in class I PurEs. A recent study of pyridinium-catalyzed mandelylthiamin decarboxylation[72] posits a direct interaction between the cationic catalyst and the decarboxylation transition state.[73]

Opportunities for Antibiotic Development. Defects in purine biosynthesis are associated with attenuated virulence in a broad range of bacterial pathogens.[74−85] PurK-knockout and (class I) PurE-knockout strains show particularly reduced pathogenicity.[81,83,86] Neither of these enzymes is found in mammals, which is the optimal situation for an antibiotic target. As demonstrated by the class-selective PurE inhibitor, 4-nitro-AIR, differences between PurE classes can be exploited despite strong mechanistic similarities. Several such differences are described here: different AIR conformations, the additional steric volume associated with the class II CO_2 portal, and the aminoimidazole ring flip that is uniquely required for formation of N^5-CAIR by class I PurE.

■ ASSOCIATED CONTENT

Supporting Information. Purine biosynthesis genes in *T. denticola* (Table S1), oligodeoxynucleotide sequences (Table S2), organism data and aligned sequences (Tables S3−S9), dendrograms for PurE (Figure S1) and PurK (Figure S2), kinetic parameters and saturation curves for *Td*PurE (Table S10 and Figures S3 and S4), stereodiagrams of superposed AIR complexes (Figure S5) and the CO_2 portal (Figure S6), the gene synthesis method (Appendix 1 and Figure S7), the derivation of the pH−rate model (Appendix 2 and Figure S8), and the N^5-CAIR recycling system (Appendix 3 and Figure S9). This material is available free of charge via the Internet at http://pubs.acs.org.

■ AUTHOR INFORMATION

Corresponding Author

*E-mail: kappock@purdue.edu. Phone: (765) 494-8383. Fax: (765) 494-1897.

Notes

[a]The same is observed in unpublished genomes of five other microbes that have class II PurE genes. All are thermophilic anaerobes or microaerophiles.

[b]No organism is known to contain both a class II PurE and a PurK. However, the absence of PurK does not by itself indicate that a class II PurE is present. Many archaeal and bacterial genomes contain a class I PurE but lack a PurK homologue (Tables S6 and S7 of the Supporting Information).

[c]The mutant protein was overproduced in *purE*-containing *E. coli*; however, contaminating host PurE should be removed by the "subtractive" hydroxyapatite step.[6]

[d]Gln109 and Arg104 differ in class I PurEs from halophilic euryarchaea and class II PurEs from insects.

[e]The ligand electron density was originally assigned as isoCAIR.[11] A later analysis showed that AIR·CO_2 is a better fit to the experimental data.[12]

Funding Sources

This work was supported by the Herman Frasch Foundation for Research in Agricultural Chemistry (531-HF02), the Pacific Enzyme Science Trust (MB-22), and Purdue University Agricultural Research Programs.

■ ACKNOWLEDGMENT

We thank J. R. Williamson and A. Beck for the *E. coli* PurC expression construct, E. A. Mullins for comments on the manuscript, and R. Stegeman and J. Nix for help with X-ray data.

■ ABBREVIATIONS

AIR, 5-aminoimidazole ribonucleotide; CAIR, 4-carboxy-AIR; N^5-CAIR, N^5-carboxy-AIR; PAICS, PurC−PurE fusion protein; *Aa*PurE, class I PurE from *A. aceti*; *Ec*PurE, class I PurE from *E. coli*; ChickE, class II PurE domain from chicken PAICS; *Td*PurE, class II PurE from *T. denticola*; NJ, neighbor-joining; ML, maximum likelihood; $[CO_2]_T$, total $[CO_2 + HCO_3^-]$; PEP, phosphoenolpyruvate; MES, 2-(*N*-morpholino)ethanesulfonic acid; CrP, creatine phosphate; CK, creatine kinase; isoCAIR,

(4*R*)-carboxy-5-iminoimidazoline ribonucleotide; yAIR, nitrogen ylide form of AIR.

REFERENCES

(1) Firestine, S. M., Poon, S. W., Mueller, E. J., Stubbe, J., and Davisson, V. J. (1994) Reactions catalyzed by 5-aminoimidazole ribonucleotide carboxylases from *Escherichia coli* and *Gallus gallus*: A case for divergent catalytic mechanisms. *Biochemistry 33*, 11927–11934.

(2) Mueller, E. J., Meyer, E., Rudolph, J., Davisson, V. J., and Stubbe, J. (1994) N^5-Carboxyaminoimidazole ribonucleotide: Evidence for a new intermediate and two new enzymatic activities in the de novo purine biosynthetic pathway of *Escherichia coli*. *Biochemistry 33*, 2269–2278.

(3) Chapman, K. A., Delauney, A. J., Kim, J. H., and Verma, D. P. (1994) Structural organization of de novo purine biosynthesis enzymes in plants: 5-Aminoimidazole ribonucleotide carboxylase and 5-aminoimidazole-4-N-succinocarboxamide ribonucleotide synthetase cDNAs from *Vigna aconitifolia*. *Plant Mol. Biol. 24*, 389–395.

(4) Firestine, S. M., Misialek, S., Toffaletti, D. L., Klem, T. J., Perfect, J. R., and Davisson, V. J. (1998) Biochemical role of the *Cryptococcus neoformans* ADE2 protein in fungal de novo purine biosynthesis. *Arch. Biochem. Biophys. 351*, 123–134.

(5) Lukens, L. N., and Buchanan, J. M. (1959) Biosynthesis of the purines. XXIV. The enzymatic synthesis of 5-amino-1-ribosyl-4-imidazolecarboxylic acid 5′-phosphate from 5-amino-1-ribosylimidazole 5′-phosphate and carbon dioxide. *J. Biol. Chem. 234*, 1799–1805.

(6) Meyer, E., Leonard, N. J., Bhat, B., Stubbe, J., and Smith, J. M. (1992) Purification and characterization of the *purE*, *purK*, and *purC* gene products: Identification of a previously unrecognized energy requirement in the purine biosynthetic pathway. *Biochemistry 31*, 5022–5032.

(7) Firestine, S. M., and Davisson, V. J. (1994) Carboxylases in de novo purine biosynthesis. Characterization of the *Gallus gallus* bifunctional enzyme. *Biochemistry 33*, 11917–11926.

(8) Meyer, E., Kappock, T. J., Osuji, C., and Stubbe, J. (1999) Evidence for the direct transfer of the carboxylate of N^5-carboxyaminoimidazole ribonucleotide (N^5-CAIR) to generate 4-carboxy-5-aminoimidazole ribonucleotide catalyzed by *Escherichia coli* PurE, an N^5-CAIR mutase. *Biochemistry 38*, 3012–3018.

(9) Mathews, I. I., Kappock, T. J., Stubbe, J., and Ealick, S. E. (1999) Crystal structure of *Escherichia coli* PurE, an unusual mutase in the purine biosynthetic pathway. *Struct. Folding Des. 7*, 1395–1406.

(10) Boyle, M. P., Kalliomaa, A. K., Levdikov, V., Blagova, E., Fogg, M. J., Brannigan, J. A., Wilson, K. S., and Wilkinson, A. J. (2005) Crystal structure of PurE (BA0288) from *Bacillus anthracis* at 1.8 Å resolution. *Proteins 61*, 674–676.

(11) Constantine, C. Z., Starks, C. M., Mill, C. P., Ransome, A. E., Karpowicz, S. J., Francois, J. A., Goodman, R. A., and Kappock, T. J. (2006) Biochemical and structural studies of N^5-carboxyaminoimidazole ribonucleotide mutase (PurE) from the acidophilic bacterium *Acetobacter aceti*. *Biochemistry 45*, 8193–8208.

(12) Hoskins, A. A., Morar, M., Kappock, T. J., Mathews, I. I., Zaugg, J. B., Barder, T. E., Peng, P., Okamoto, A., Ealick, S. E., and Stubbe, J. (2007) N^5-CAIR mutase: Role of a CO_2 binding site and substrate movement in catalysis. *Biochemistry 46*, 2842–2855.

(13) Li, S. X., Tong, Y. P., Xie, X. C., Wang, Q. H., Zhou, H. N., Han, Y., Zhang, Z. Y., Gao, W., Li, S. G., Zhang, X. C., and Bi, R. C. (2007) Octameric structure of the human bifunctional enzyme PAICS in purine biosynthesis. *J. Mol. Biol. 366*, 1603–1614.

(14) Grenier, D. (1992) Nutritional interactions between two suspected periodontopathogens, *Treponema denticola* and *Porphyromonas gingivalis*. *Infect. Immun. 60*, 5298–5301.

(15) Riviere, G. R., Elliot, K. S., Adams, D. F., Simonson, L. G., Forgas, L. B., Nilius, A. M., and Lukehart, S. A. (1992) Relative proportions of pathogen-related oral spirochetes (PROS) and *Treponema denticola* in supragingival and subgingival plaque from patients with periodontitis. *J. Periodontol. 63*, 131–136.

(16) Takeuchi, Y., Umeda, M., Sakamoto, M., Benno, Y., Huang, Y., and Ishikawa, I. (2001) *Treponema socranskii*, *Treponema denticola*, and *Porphyromonas gingivalis* are associated with severity of periodontal tissue destruction. *J. Periodontol. 72*, 1354–1363.

(17) Fraser, C. M. et al. (1997) Genomic sequence of a Lyme disease spirochaete, *Borrelia burgdorferi*. *Nature 390*, 580–586.

(18) Fraser, C. M. et al. (1998) Complete genome sequence of *Treponema pallidum*, the syphilis spirochete. *Science 281*, 375–388.

(19) Ren, S. X. et al. (2003) Unique physiological and pathogenic features of *Leptospira interrogans* revealed by whole-genome sequencing. *Nature 422*, 888–893.

(20) Seshadri, R. et al. (2004) Comparison of the genome of the oral pathogen *Treponema denticola* with other spirochete genomes. *Proc. Natl. Acad. Sci. U.S.A. 101*, 5646–5651.

(21) Bradford, M. M. (1976) A rapid and sensitive method for the quantitation of microgram quantities of protein utilizing the principle of protein-dye binding. *Anal. Biochem. 72*, 248–254.

(22) Schultheisz, H. L., Szymczyna, B. R., Scott, L. G., and Williamson, J. R. (2008) Pathway engineered enzymatic de novo purine nucleotide synthesis. *ACS Chem. Biol. 3*, 499–511.

(23) Srivastava, P. C., Mancuso, R. W., Rousseau, R. J., and Robins, R. K. (1974) Nucleoside peptides. 6. Synthesis of certain N-(5-amino-1-(β-D-ribofuranosyl)imidazole-4-carbonyl)amino acids related to naturally occurring intermediates in the purine biosynthetic pathway. *J. Med. Chem. 17*, 1207–1211.

(24) Thompson, J. D., Higgins, D. G., and Gibson, T. J. (1994) CLUSTAL W: Improving the sensitivity of progressive multiple sequence alignment through sequence weighting, position-specific gap penalties and weight matrix choice. *Nucleic Acids Res. 22*, 4673–4680.

(25) Tamura, K., Dudley, J., Nei, M., and Kumar, S. (2007) MEGA4: Molecular Evolutionary Genetics Analysis (MEGA) Software Version 4.0. *Mol. Biol. Evol. 24*, 1596–1599.

(26) Hall, B. G. (2005) Comparison of the accuracies of several phylogenetic methods using protein and DNA sequences. *Mol. Biol. Evol. 22*, 792–802.

(27) Felsenstein, J. (1985) Confidence limits on phylogenies: An approach using the bootstrap. *Evolution 39*, 783–791.

(28) Saitou, N., and Nei, M. (1987) The neighbor-joining method: A new method for reconstructing phylogenetic trees. *Mol. Biol. Evol. 4*, 406–425.

(29) Zuckerkandl, E., and Pauling, L. (1965) Molecules as documents of evolutionary history. *J. Theor. Biol. 8*, 357–366.

(30) Felsenstein, J. (1981) Evolutionary trees from DNA sequences: A maximum likelihood approach. *J. Mol. Evol. 17*, 368–376.

(31) Galtier, N., Gouy, M., and Gautier, C. (1996) SEAVIEW and PHYLO_WIN: Two graphic tools for sequence alignment and molecular phylogeny. *Comput. Appl. Biosci. 12*, 543–548.

(32) Studier, F. W. (2005) Protein production by auto-induction in high density shaking cultures. *Protein Expression Purif. 41*, 207–234.

(33) Ellis, K. J., and Morrison, J. F. (1982) Buffers of constant ionic strength for studying pH-dependent processes. *Methods Enzymol. 87*, 405–426.

(34) Dean, J. A. (1979) *Lange's handbook of chemistry*, 12th ed., McGraw-Hill, New York.

(35) Teng, T.-Y. (1990) Mounting of crystals for macromolecular crystallography in a free-standing thin film. *J. Appl. Crystallogr. 23*, 387–391.

(36) Pflugrath, J. W. (1999) The finer things in X-ray diffraction data collection. *Acta Crystallogr. D55*, 1718–1725.

(37) Schwarzenbacher, R. et al. (2004) Crystal structure of a phosphoribosylaminoimidazole mutase PurE (TM0446) from *Thermotoga maritima* at 1.77-Å resolution. *Proteins 55*, 474–478.

(38) Kleywegt, G. J., and Jones, T. A. (1996) Making the most of your search model. *CCP4/ESF-EACBM Newsletter on Protein Crystallography 32*, 32–36.

(39) Vagin, A., and Teplyakov, A. (1997) MOLREP: An automated program for molecular replacement. *J. Appl. Crystallogr. 30*, 1022–1025.

(40) Brünger, A. T., Adams, P. D., Clore, G. M., DeLano, W. L., Gros, P., Grosse-Kunstleve, R. W., Jiang, J. S., Kuszewski, J., Nilges, M.,

Pannu, N. S., Read, R. J., Rice, L. M., Simonson, T., and Warren, G. L. (1998) Crystallography & NMR system: A new software suite for macromolecular structure determination. *Acta Crystallogr. D54*, 905–921.

(41) Jones, T. A., Zou, J. Y., Cowan, S. W., and Kjeldgaard, M. (1991) Improved methods for building protein models in electron density maps and the location of errors in these models. *Acta Crystallogr. A47*, 110–119.

(42) Vagin, A. A., Steiner, R. A., Lebedev, A. A., Potterton, L., McNicholas, S., Long, F., and Murshudov, G. N. (2004) REFMAC5 dictionary: Organization of prior chemical knowledge and guidelines for its use. *Acta Crystallogr. D60*, 2184–2195.

(43) Perrakis, A., Sixma, T. K., Wilson, K. S., and Lamzin, V. S. (1997) wARP: Improvement and extension of crystallographic phases by weighted averaging of multiple-refined dummy atomic models. *Acta Crystallogr. D53*, 448–455.

(44) Yeates, T. O. (1988) Simple statistics for intensity data from twinned specimens. *Acta Crystallogr. A44*, 142–144.

(45) Collaborative Computational Project, Number 4. (1994) The CCP4 suite: Programs for protein crystallography. *Acta Crystallogr. D50*, 760–770.

(46) Kabsch, W. (2010) XDS. *Acta Crystallogr. D66*, 125–132.

(47) Murshudov, G. N., Skubák, P., Lebedev, A. A., Pannu, N. S., Steiner, R. A., Nicholls, R. A., Winn, M. D., Long, F., and Vagin, A. A. (2011) *REFMAC5* for the refinement of macromolecular crystal structures. *Acta Crystallogr. D67*, 355–367.

(48) Emsley, P., Lohkamp, B., Scott, W. G., and Cowtan, K. (2010) Features and development of Coot. *Acta Crystallogr. D66*, 486–501.

(49) Kleywegt, G. J. (1996) Use of non-crystallographic symmetry in protein structure refinement. *Acta Crystallogr. D52*, 842–857.

(50) DeLano, W. L. (2002) *The PyMOL Molecular Graphics System*, DeLano Scientific, San Carlos, CA.

(51) Gouet, P., Courcelle, E., Stuart, D. I., and Metoz, F. (1999) ESPript: Analysis of multiple sequence alignments in PostScript. *Bioinformatics 15*, 305–308.

(52) Thoden, J. B., Kappock, T. J., Stubbe, J., and Holden, H. M. (1999) Three-dimensional structure of N^5-carboxyaminoimidazole ribonucleotide synthetase: A member of the ATP grasp protein superfamily. *Biochemistry 38*, 15480–15492.

(53) Lerman, C. L., and Cohn, M. (1980) ^{31}P NMR quantitation of the displacement of equilibria of arginine, creatine, pyruvate, and 3-P-glycerate kinase reactions by substitution of sulfur for oxygen in the β phosphate of ATP. *J. Biol. Chem. 255*, 8756–8760.

(54) Morrison, J. F., and White, A. (1967) Isotope exchange studies of the reaction catalyzed by ATP:creatine phosphotransferase. *Eur. J. Biochem. 3*, 145–152.

(55) Teague, W. E., Jr., and Dobson, G. P. (1992) Effect of temperature on the creatine kinase equilibrium. *J. Biol. Chem. 267*, 14084–14093.

(56) Crans, D. C., Kazlauskas, R. J., Hirschbein, B. L., Wong, C.-H., Abril, O., and Whitesides, G. M. (1987) Enzymatic regeneration of adenosine 5′-triphosphate: Acetyl phosphate, phosphoenolpyruvate, methoxycarbonyl phosphate, dihydroxyacetone phosphate, 5-phospho-α-D-ribosyl pyrophosphate, uridine-5′-diphosphoglucose. *Methods Enzymol. 136*, 263–280.

(57) Meyer, E. (1996) Two new activities and a new intermediate in the purine pathway. Ph.D. Thesis, Massachusetts Institute of Technology, Cambridge, MA.

(58) Cooper, T. G., Tchen, T. T., Wood, H. G., and Benedict, C. R. (1968) The carboxylation of phosphoenolpyruvate and pyruvate. I. The active species of "CO_2" utilized by phosphoenolpyruvate carboxykinase, carboxytransphosphorylase, and pyruvate carboxylase. *J. Biol. Chem. 243*, 3857–3863.

(59) Klengel, T., Liang, W.-J., Chaloupka, J., Ruoff, C., Schröppel, K., Naglik, J. R., Eckert, S. E., Mogensen, E. G., Haynes, K., Tuite, M. F., Levin, L. R., Buck, J., and Mühlschlegel, F. A. (2005) Fungal adenylyl cyclase integrates CO_2 sensing with cAMP signaling and virulence. *Curr. Biol. 15*, 2021–2026.

(60) Burghout, P., Cron, L. E., Gradstedt, H., Quintero, B., Simonetti, E., Bijlsma, J. J. E., Bootsma, H. J., and Hermans, P. W. M. (2010) Carbonic anhydrase is essential for *Streptococcus pneumoniae* growth in environmental ambient air. *J. Bacteriol. 192*, 4054–4062.

(61) Merlin, C., Masters, M., McAteer, S., and Coulson, A. (2003) Why is carbonic anhydrase essential to *Escherichia coli*?. *J. Bacteriol. 185*, 6415–6424.

(62) Smith, K. S., Jakubzick, C., Whittam, T. S., and Ferry, J. G. (1999) Carbonic anhydrase is an ancient enzyme widespread in prokaryotes. *Proc. Natl. Acad. Sci. U.S.A. 96*, 15184–15189.

(63) Holland, H. D., Lazar, B., and McCaffrey, M. (1986) Evolution of the atmosphere and oceans. *Nature 320*, 27–33.

(64) Sheldon, N. D. (2006) Precambrian paleosols and atmospheric CO_2 levels. *Precambrian Res. 147*, 148–155.

(65) Litchfield, G. J., and Shaw, G. (1971) Purines, pyrimidines, and imidazoles. Part XXXVIII. A kinetic study of the decarboxylation of 5-amino-1-β-D-ribofuranosylimidazole-4-carboxylic acid 5′-phosphate and related compounds. *J. Chem. Soc. B*, 1474–1484.

(66) Bhat, B., Groziak, M. P., and Leonard, N. J. (1990) Nonenzymatic synthesis and properties of 5-aminoimidazole ribonucleotide (AIR). Synthesis of specifically ^{15}N-labeled 5-aminoimidazole ribonucleoside (AIRs) derivatives. *J. Am. Chem. Soc. 112*, 4891–4897.

(67) Dunn, G. E., Thimm, H. F., and Mohanty, R. K. (1979) Kinetics and mechanism of decarboxylation of some pyridinecarboxylic acids in aqueous solution. III. 3-Hydroxy- and 3-aminopyridine-2-carboxylic acids. *Can. J. Chem. 57*, 1098–1104.

(68) Amyes, T. L., Wood, B. M., Chan, K., Gerlt, J. A., and Richard, J. P. (2008) Formation and stability of a vinyl carbanion at the active site of orotidine 5′-monophosphate decarboxylase: pK_a of the C-6 proton of enzyme-bound UMP. *J. Am. Chem. Soc. 130*, 1574–1575.

(69) Firestine, S. M., Wu, W., Youn, H., and Davisson, V. J. (2009) Interrogating the mechanism of a tight binding inhibitor of AIR carboxylase. *Bioorg. Med. Chem. 17*, 794–803.

(70) Firestine, S. M., and Davisson, V. J. (1993) A tight binding inhibitor of 5-aminoimidazole ribonucleotide carboxylase. *J. Med. Chem. 36*, 3484–3486.

(71) Bláievic, N., Kajfež, F., and Šunjic¢, V. (1970) σ Values of some nitroimidazoles. *J. Heterocycl. Chem. 7*, 227–229.

(72) Kluger, R., Ikeda, G., Hu, Q., Cao, P., and Drewry, J. (2006) Accelerating unimolecular decarboxylation by preassociated acid catalysis in thiamin-derived intermediates: Implicating Brønsted acids as carbanion traps in enzymes. *J. Am. Chem. Soc. 128*, 15856–15864.

(73) Gonzalez-James, O. M., and Singleton, D. A. (2010) Isotope effect, mechanism, and origin of catalysis in the decarboxylation of mandelylthiamin. *J. Am. Chem. Soc. 132*, 6896–6897.

(74) Levine, H. B., and Maurer, R. L. (1958) Immunization with an induced avirulent auxotrophic mutant of *Pseudomonas pseudomallei*. *J. Immunol. 81*, 433–438.

(75) Ivánovics, G., Marjai, E., and Dobozy, A. (1968) The growth of purine mutants of *Bacillus anthracis* in the body of the mouse. *J. Gen. Microbiol. 53*, 147–162.

(76) Baselski, V. S., Upchurch, S., and Parker, C. D. (1978) Isolation and phenotypic characterization of virulence-deficient mutants of *Vibrio cholerae*. *Infect. Immun. 22*, 181–188.

(77) Straley, S. C., and Harmon, P. A. (1984) Growth in mouse peritoneal macrophages of *Yersinia pestis* lacking established virulence determinants. *Infect. Immun. 45*, 649–654.

(78) Fields, P. I., Swanson, R. V., Haidaris, C. G., and Heffron, F. (1986) Mutants of *Salmonella typhimurium* that cannot survive within the macrophage are avirulent. *Proc. Natl. Acad. Sci. U.S.A. 83*, 5189–5193.

(79) McFarland, W. C., and Stocker, B. A. D. (1987) Effect of different purine auxotrophic mutations on mouse-virulence of a Vi-positive strain of *Salmonella dublin* and of two strains of *Salmonella typhimurium*. *Microb. Pathog. 3*, 129–141.

(80) Mahan, M. J., Slauch, J. M., and Mekalanos, J. J. (1993) Selection of bacterial virulence genes that are specifically induced in host tissues. *Science 259*, 686–688.

(81) Alcantara, R. B., Read, R. D. A., Valderas, M. W., Brown, T. D., and Roop, R. M. (2004) Intact purine biosynthesis pathways are

required for wild-type virulence of *Brucella abortus* 2308 in the BALB/c mouse model. *Infect. Immun. 72*, 4911–4917.

(82) Pechous, R., Celli, J., Penoske, R., Hayes, S. F., Frank, D. W., and Zahrt, T. C. (2006) Construction and characterization of an attenuated purine auxotroph in a *Francisella tularensis* live vaccine strain. *Infect. Immun. 74*, 4452–4461.

(83) Samant, S., Lee, H., Ghassemi, M., Chen, J., Cook, J. L., Mankin, A. S., and Neyfakh, A. A. (2008) Nucleotide biosynthesis is critical for growth of bacteria in human blood. *PLoS Pathog. 4*, e37.

(84) Lan, L., Cheng, A., Dunman, P. M., Missiakas, D., and He, C. (2010) Golden pigment production and virulence gene expression are affected by metabolisms in *Staphylococcus aureus*. *J. Bacteriol. 192*, 3068–3077.

(85) Propst, K. L., Mima, T., Choi, K.-H., Dow, S. W., and Schweizer, H. P. (2010) A *Burkholderia pseudomallei* D *purM* mutant is avirulent in immunocompetent and immunodeficient animals: candidate strain for exclusion from select-agent lists. *Infect. Immun. 78*, 3136–3143.

(86) Crawford, R. M., Van De Verg, L., Yuan, L., Hadfield, T. L., Warren, R. L., Drazek, E. S., Houng, H. H., Hammack, C., Sasala, K., Polsinelli, T., Thompson, J., and Hoover, D. L. (1996) Deletion of *purE* attenuates *Brucella melitensis* infection in mice. *Infect. Immun. 64*, 2188–2192.